

# 1 **Baltic Sea Surface Temperature Analysis 2022: A Study of Marine** 2 **Heatwaves and Overall High Seasonal Temperatures**

3 Anja Lindenthal<sup>1</sup> and Claudia Hinrichs<sup>1</sup>, Simon Jandt-Scheelke<sup>1</sup>, Tim Kruschke<sup>1</sup>, Priidik Lagemaa<sup>3</sup>, Eefke  
4 M. van der Lee<sup>2</sup>, Ilja Maljutenko<sup>3</sup>, Helen E. Morrison<sup>2</sup>, Tabea R. Panteleit<sup>1</sup>, Urmas Raudsepp<sup>3</sup>

5 <sup>1</sup>Federal Maritime and Hydrographic Agency, Hamburg, 20539, Germany

6 <sup>2</sup>Federal Maritime and Hydrographic Agency, Rostock, 18057, Germany

7 <sup>3</sup>Department of Marine Systems, Tallinn University of Technology, Tallinn, 12618, Estonia

8 *Correspondence to:* Claudia Hinrichs ([claudia.hinrichs@bsh.de](mailto:claudia.hinrichs@bsh.de)); Helen E. Morrison ([helen.morrison@bsh.de](mailto:helen.morrison@bsh.de))

9 **Abstract.** In 2022, large parts of the Baltic Sea surface experienced the third-warmest to the warmest temperatures over the  
10 summer and autumn months since 1997. Warm temperature anomalies can lead to marine heatwaves (MHWs), which are  
11 discrete periods of anomalous high temperatures relative to the usual local conditions. Here, we describe the overall sea surface  
12 temperature (SST) conditions observed in the Baltic Sea in 2022 and provide a spatio-temporal description of surface MHW  
13 events based on remote sensing, model reanalyses and in-situ station data. The most MHWs, locally up to seven MHW events,  
14 were detected in the western Baltic Sea and the Inner Danish Straits, where maximum MHW intensities reached values of up  
15 to 4.6 °C above the climatological mean. The northern Baltic Proper and the Gulf of Bothnia were impacted mainly by two  
16 MHWs at maximum intensities of 7.3 °C and 9.6 °C, respectively. Our results also reveal that MHWs in the upper layer occur  
17 at a different period than at the bottom layers and are likely driven by different mechanisms. Model data from two exemplary  
18 stations, ‘Lighthouse Kiel (LT Kiel)’ and ‘Northern Baltic’, show a significant increase in MHW occurrences, of +0.73 MHW  
19 events per decade at LT Kiel and of +0.64 MHW events per decade at Northern Baltic, between 1993 and 2022. Moreover, we  
20 discuss the expected future increased occurrence of MHWs based on a statistical analysis at both locations.

## 21 **1 Introduction**

22 Global warming has led to an increase of ocean heat content (OHC) by about 350 ZJ in the upper 2000 meters from 1958 to  
23 2019, with the year 2022 being the warmest on record as of this writing (Cheng et al., 2022; WMO, 2023). Simultaneously,  
24 marine heatwaves (MHWs), extreme events of high water temperature (Hobday et al., 2016), have increased in frequency,  
25 duration, spatial extent and intensity during the past four decades (Sun et al., 2023). In 2022, MHWs were recorded on 58 %  
26 of the ocean surface (WMO, 2023).

27 The Baltic Sea is one of the marine ecosystems with the fastest recorded warming of surface temperatures of 1.35 °C between  
28 1982 and 2006, i.e., 0.54 °C per decade (Belkin, 2009). SST data operationally produced by the German Federal Maritime and  
29 Hydrographic Agency (in the following BSH, product ref. no. 1 in Table 1) show a warming trend of 0.58 °C per decade for

30 the period 1990–2022. High SSTs can affect phytoplankton production, while unprecedented high temperatures in the  
31 subsurface layers of the sea could have even more devastating effects on the marine ecosystem (Kauppi et al., 2023).  
32 Conditions that facilitate the fast warming of the Baltic Sea are the limited exchange between surface and deeper layers due to  
33 a permanent halocline at a depth of 60–80 m (Väli et al., 2013) and the limited water exchange between the Baltic Sea and the  
34 open ocean through the narrow Skagerrak. That is why local air-sea heat exchange is the main physical factor for the surface  
35 layer water temperature and heat content in the Baltic Sea (Raudsepp et al., 2022).

36 Global mean air temperature in 2022 was among the six warmest in the 173-year instrumental record (WMO, 2023). For  
37 Europe especially, the Copernicus Climate Change Service/ECMWF (2022a) states that the air temperatures in August 2022  
38 were higher than the 1991–2020 average across most of the continent, especially in a band in Eastern Europe stretching from  
39 the Barents and Kara seas to the Caucasus. In November 2022, air temperatures were higher than the 1991–2020 average,  
40 especially over the west, south-east and far north of Europe, and were unusually mild over the northern European seas  
41 (Copernicus Climate Change Service/ECMWF, 2022b). These large-scale weather patterns likely lead to high sea surface  
42 temperatures (SST) in marginal seas like the Baltic Sea and are a likely driver of MHWs. This hypothesis is further supported  
43 by a study by Holbrook et al. (2019), which found that MHWs at middle and high latitude regions were driven by large-scale  
44 atmospheric pressure anomalies which cause anomalous ocean warming. Stalled atmospheric high-pressure systems coincide  
45 with clear skies, warm air, and reduced wind speeds. These conditions then lead to quick warming of the upper ocean and  
46 increased thermal stratification due to reduced vertical mixing.

47 So far, there generally have been only a few studies on MHWs in the Baltic Sea (Goebeler et al., 2022; She et al., 2020). In  
48 this study, we show that remote sensing data revealed several SST anomalies over the entire Baltic Sea in 2022. We thus use  
49 model reanalysis and in-situ station data to provide a spatio-temporal description of the corresponding MHWs. Both datasets  
50 contain data collected over a long enough period to also provide its own respective climatology, thereby enabling a consistent  
51 representation of MHWs. While the in-situ data provides accurate point-wise measurements of the temperature at selected  
52 locations, the model reanalysis data allows for a widespread analysis of MHWs over the entire Baltic Sea, including their  
53 extension into subsurface layers. Furthermore, we extend our study by providing a climatology of MHWs at two specific  
54 mooring locations, namely at the Lighthouse Kiel (LT Kiel) and Northern Baltic stations. The overall aim of this study is to  
55 highlight the areas of the Baltic Sea that were (most) affected by MHWs and determine whether surface MHWs can propagate  
56 into deeper layers and thus potentially threaten the subsurface ecosystem. Furthermore, analyzing the climatology of MHWs  
57 can provide insight into whether the global increase in MHWs can also be expected to occur on a local scale for the Baltic Sea.

## 58 **2 Data and Methods**

### 59 **2.1 Satellite data**

60 The satellite data service at the BSH compiles daily maps of SST data (product ref. no. 1 in Table 1). These have contributed  
61 for example to studies by the BACC Author Team (2008) and Gröger et al. (2022). The SST data are recorded as radiances by  
62 the Advanced Very High Resolution Radiometer (AVHRR/3) in two thermal infrared channels aboard the NOAA-19 and  
63 MetOp B satellites, providing a spatial resolution of 1.1 km, swath widths of 1,447 km and orbital periods of 100 minutes  
64 (EUMETSAT, 2015; Minnett et al., 2019). The raw data of eight or nine daytime passes over the Baltic and North Sea are  
65 received directly from EUMETSAT and processed using automated, standardized correction procedures (atmospheric  
66 correction, cloud masking, georeferencing etc.). Additionally, each flyover is corrected manually in order to preserve as much  
67 data as possible whilst eliminating any faulty or cloudy pixels. All available single images from a calendar day are combined  
68 and averaged, on a single pixel basis, into one daily-mean image. These daily images are then used to produce a weekly  
69 analysis on an operational basis. While the BSH has been carrying out the processing of the satellite data itself on the 1.1 km  
70 grid since 1990, operational SST analysis for the Baltic Sea did not start until the autumn of 1996. The analysis of the BSH  
71 SST dataset presented in this chapter is therefore limited to the period from 1997–2022.

### 72 **2.2 Station data**

73 In-situ temperature time series from mooring stations located in the Baltic Sea are used for 1) model validation and 2) cross  
74 validation of the MHW computation from model data. Except for SST data from Northern Baltic (K. Hedi, FMI, pers.  
75 communication), the station data are obtained from product ref. no. 2 in Table 1. Each available dataset has already been  
76 quality controlled by the regional production units (In Situ TAC partners, 2022). The temporal resolution varies from hourly  
77 at the German stations to half-hourly at the stations in the northern Baltic Proper and Gulf of Finland. Due to failures,  
78 maintenance and other circumstances, no mooring station entirely covers the period from 1st Jan 1993 until now.  
79 Of all available mooring stations, we selected those which contain data from 2022 and from at least ten additional years from  
80 1993 until 2021 at least one depth. Out of the remaining seven mooring stations that contained surface temperature data, two  
81 mooring stations were chosen for the cross validation of MHWs: Lighthouse Kiel (LT Kiel) and Northern Baltic (Fig. 1). Of  
82 the observation data, LT Kiel has the greatest time coverage (1989 until the present, missing data: 9.1 % of days). This mooring  
83 station lies in the far western part of the southern Baltic, and the water depth there is about 12 m. The station Northern Baltic  
84 is located in the northern Baltic Proper. The SST observations there cover the period from 1997 until now (missing data: 8.0 %  
85 of days). No mooring station provides a time series in deeper layers long or consistent enough to analyze subsurface MHWs,  
86 thus reducing the scope of measurement-based analysis of MHWs to the surface layers.

## 87 **2.3 Baltic Sea Physics Reanalysis Data**

88 The Baltic Sea physics reanalysis product (product ref. no. 3 in Table 1) is a model dataset based on the ocean model NEMO  
89 v4.0 (Gurvan et al., 2019). The model system assimilates satellite observations of SST (EU Copernicus Marine Service  
90 Product, 2022b) and in-situ temperature and salinity profile observations from the ICES database (ICES Bottle and low-  
91 resolution CTD dataset, 2022). The product provides gridded information on SST and subsurface temperature conditions. The  
92 spatial coverage is 1 nautical mile, i.e., approximately 1.8 km. The grid covers the entire Baltic Sea, including the transition  
93 zone to the North Sea, with a vertical resolution of 56 non-equidistant depth levels. This multi-year product (MYP) covers the  
94 reference period from 1993 up to 2022. The model setup is described in the Product User Manual (PUM, Ringgaard et al.,  
95 2023).

## 96 **2.4 Heat wave detection**

97 Marine heatwaves refer to a discrete period of unusually high seawater temperatures. While several definitions describe MHWs  
98 quantitatively, the most commonly used method defines them as periods when temperatures exceed the 90th percentile of the  
99 local climatology for five days or more (Hobday et al. 2016). We use open-source tools to detect MHWs (Oliver, 2016; Zhao  
100 and Marin, 2019) in station and model data. The identified MHWs can be classified following Hobday et al. (2018), in which  
101 the MHW category is based on the maximum intensity in multiples of threshold exceedances, i.e., the local difference between  
102 the 90th percentile threshold and the climatology. If the threshold is exceeded less than 2 times, the MHW is classified as  
103 moderate (Category I), at 2 to 3 times it is classified as strong (Category II), at 3 to 4 times it is classified as severe (Category  
104 III), and at 4 or more times it is classified as extreme (Category IV).

105 Here, the occurrence of MHWs in the Baltic Sea in 2022 is analyzed based on the Baltic Sea MYP (product ref. no 3 in Table  
106 1). The following statistical metrics of MHWs are computed at every third surface grid point of the MYP, resulting in a  
107 resolution of approximately 5.4 km: cumulative intensity, mean intensity, duration of the longest heatwave, number of  
108 heatwaves (frequency), maximum intensity and total days of MHW conditions.

109 Then, in order to evaluate the development of those MHW metrics over time, block averages (using a block length of one year)  
110 for each MHW metric are computed for both the observations (product ref. no 2 in Table 1) and the model data (product ref.  
111 no 3 in Table 1) at two stations: Lighthouse Kiel and Northern Baltic. The yearly MHW metrics from observations and the  
112 model are correlated for evaluation, and linear trends (95 % significance) are calculated for each of those metrics. Finally, the  
113 correlation of the annual MHW metrics to the annual mean temperature based on model data was assessed using a linear least-  
114 squares regression and a two-sided t-test for significance.

115 All MHW assessments in the following sections use the period from 1993 to 2021 for the climatology, except for Sect. 3.2.1,  
116 in which the comparison of the multi-year evolution of MHWs at Northern Baltic uses the overlapping period from 1997 to  
117 2021 due to the lack of observations at this station before 1997.

## 118 2.5 Model validation

119 The MYP data has already been extensively validated in the corresponding Quality Information Document (QuID; Panteleit  
120 et al., 2023). In this document, the MYP data are validated within the time period from 1st January 1993 to 31st December  
121 2018. The validation shows a negative bias at the surface with a shift towards more positive values at deeper levels. A variation  
122 of statistical values with depth is also clearly visible in the estimated accuracy number (EAN), which represents the root-mean  
123 square difference (RMSD) of a specific depth layer. The RMSD varies between 0.29 °C at 200–400 m over 0.63 °C at the  
124 surface to 1.3 °C at 5–30 m depth.

125 We additionally evaluated the model data in more detail using a clustering approach, which offers insights into the overall  
126 accuracy of the model by grouping the errors. This clustering procedure employs the K-means algorithm (Raudsepp and  
127 Maljutenko, 2022). In this evaluation, all available data within the model's domain and simulation period are considered. A  
128 two-dimensional error space ( $dS$ ,  $dT$ ) is established using simultaneously measured temperature and salinity values as the  
129 foundation for clustering. Here,  $dS=(S_{\text{mod}}-S_{\text{obs}})$  and  $dT=(T_{\text{mod}}-T_{\text{obs}})$  represent the differences between the model ( $S_{\text{mod}}$  and  $T_{\text{mod}}$ )  
130 and observed ( $S_{\text{obs}}$  and  $T_{\text{obs}}$ ) salinity and temperature, respectively. The dataset employed in this validation study was sourced  
131 from the EMODNET dataset compiled by SMHI (product ref. no. 4 in Table 1). It consists of a total of 3,094,089 observations  
132 aligning with the simulation period of the Baltic Sea physics reanalysis (product ref. no. 3 in Table 1) and covering the years  
133 1993 to 2022. A comprehensive explanation of the k-means-method and detailed results describing the model's accuracy can  
134 be found in Appendix A1. The results can be summarized as in that approximately 82 % of all validation points exhibit  
135 relatively low temperature bias, STD, and RMSD (Table A1). The surface layer validation shows that less than 10 % of  
136 comparison points have significant temperature errors (Figure A1c). Due to the low proportion of these validation points we  
137 do not expect a significant impact on the determination of the surface MHWs and their statistics. Below the surface layer, i.e.,  
138 at depths ranging from 0.5–40 m, up to 25 % of the points correspond to clusters with temperature errors greater than +/-  
139 2.0 °C; in deeper layers, this percentage gets smaller again (Figure A1c). Consequently, we anticipate that the model reanalysis  
140 data provide sufficiently accurate information for calculating subsurface MHWs and their statistics for the Baltic Sea as well.  
141 The model is also validated in terms of how accurately it reproduces the MHWs of 2022 and how well it represents their  
142 characteristics during the overlapping time periods of data availability at the two locations (1993–2022 for LT Kiel, and 1997–  
143 2022 for Northern Baltic). For this, the model data was compared to the available station data (product ref. no 2 in Table 1 for  
144 LT Kiel and K. Hedi, FMI, pers. communication for Northern Baltic) at these locations. Table 2 shows the Pearson correlation  
145 coefficients for the MHW metrics in Fig 4 between observational and model data for the two stations, which show overall  
146 good agreement between the model and the observation data with respect to MHW detection.

147 We also compared the annual temperature curves resulting from both the model and the station data at each location (Fig. A2).  
148 Overall, the curves show the same progression. The temperature from the MYP is generally slightly lower, and consequently  
149 this results in a slightly lower temperature climatology and threshold (here, the 90th percentile) on which MHW detection is

150 based. In general, though, the MHWs and their respective intensities and lengths are detected equally in both the station and  
151 model data.

## 152 **3 Results**

### 153 **3.1 Sea surface temperature anomalies in satellite data**

154 In the summer of 2022, large parts of the Baltic Sea featured strong warm anomalies based on the BSH SST analysis (product  
155 ref. no. 1 in Table 1, Fig. 2). The highest values were up to 3 °C above the long-term mean (1997–2021) in the Bothnian Sea  
156 in June and in the Bothnian Bay in July. In August however, these areas were neutral or exhibited cold anomalies, while the  
157 Baltic Proper as well as the Gulf of Finland and the Gulf of Riga showed the warmest anomalies of +1.5 °C to 2.5 °C. At the  
158 beginning of autumn, the Baltic Sea is marked by a substantial east-to-west gradient of SST anomalies due to a series of  
159 upwelling events along its eastern shores. In November, the whole Baltic Sea features strong warm anomalies, again with peak  
160 values above +2 °C around Southern Sweden.

161 To provide some climatological context for the observed SST anomalies in a straightforward way, we also present maps  
162 ranking the SST anomalies for the summer and autumn months of 2022 against the same months in previous years (right two  
163 columns of Fig. 2). These anomaly rankings provide information on how extreme an anomaly of a given magnitude is. For  
164 every grid point and for each calendar month, the monthly anomalies are ranked by magnitude. The warm anomalies over  
165 large parts of the Baltic Sea during the summer and autumn of 2022 are among the warmest eight on record for the respective  
166 months. In September, coastal upwelling led to cold anomalies along the eastern shores, but the other five months of the  
167 summer and fall of 2022 (June, July and August as well as October and November) show large areas of the Baltic Sea with  
168 warm anomalies that are among the four most pronounced on record. In August and November, we see several large areas  
169 along the coastlines of the Baltic countries as well as off the Polish coast and around Gotland that according to the BSH SST  
170 analysis dataset featured highest-ever surface temperatures.

### 171 **3.2 Marine heatwaves**

172 MHWs describe exceptionally warm temperature anomalies. As the monthly overview in Fig. 2 already provides an indication  
173 of possible MHW conditions in 2022, the MHW metrics defined by Hobday et al. (2016) are assessed using the Baltic Sea  
174 MYP (product ref. no. 3 in Table 1). Each region of the Baltic Sea experienced different MHW characteristics during 2022  
175 (Fig. 3, Table 3).

176 The most MHWs during 2022 occurred in the Inner Danish Straits and the Western Baltic (Fig. 3d); mainly, four to five MHWs  
177 were detected, with some assessed locations experiencing up to seven MHWs and a maximum of 94 total days of MHW  
178 conditions (Fig. 3f). The mean and maximum intensities of all MHWs in the Western Baltic reached up to 3.8 °C and 4.6 °C,  
179 respectively (Fig. 3b and 3e). The highest mean and maximum intensity values were reached in the northern Baltic Proper and

180 in the Bothnian Sea and Bothnian Bay (Fig. 3b and 3e), though these regions were affected mainly by only two MHWs. The  
181 maximum intensity in the Bothnian Bay even reached 9.6 °C, the highest within the entire studied period from 1993 to 2022.  
182 The longest MHW is found in the Baltic Proper (32 days), followed by the Bothnian Sea (31 days) and the Inner Danish Straits  
183 (29 days) (Fig. 3c). The highest values of cumulative intensity (of a single MHW), with up to 119.3 days °C, are found in the  
184 Kvarken, a strait between the Bothnian Sea and the Bothnian Bay (Fig. 3a).

### 185 **3.2.1 Multi-year evaluation of MHW metrics**

186 Next, we assess the frequency and other characteristics of the MHWs that occurred in 2022 in a climatological context based  
187 on both observations and model data for the two stations, LT Kiel (based on the overlapping climatology period 1993–2021,  
188 Fig. 4a–h) and Northern Baltic (based on the overlapping climatology period 1997–2021, Fig. 4 i–p). Overall, the results for  
189 the yearly MHW metric calculation are well correlated between the observations and the model data (Table 2).

190 In 2022, a total of five MHWs (four in the MYP) occurred throughout the year at LT Kiel (Fig. A2a). Though none of them  
191 was extraordinarily long or intense at LT Kiel, the time series of yearly MHW metrics shows that, based on observational data,  
192 the number of MHW occurrences in 2022 was the second highest there since 1989 (Fig. 4a). The time series of MHW  
193 frequencies per year suggests that the occurrence of MHW events has increased over the last three decades (Fig. 4a). The trend  
194 computed from model data is +0.73 MHWs per decade for the period 1993–2022. The number of MHW events per year is  
195 positively correlated ( $R=0.76$ ) with the increasing annual mean SST at this mooring station (Fig. 4b). The maximum (Fig. 4c)  
196 and cumulative intensities (Fig. 4e) of observed MHWs do not show a clear trend and are not correlated to the warming annual  
197 mean temperatures (Fig. 4d and Fig. 4f). There is no significant trend in total MHW days (Fig. 4g) at LT Kiel, but a positive  
198 correlation ( $R=0.71$ ) with rising average temperatures (Fig. 4h).

199 For Northern Baltic, neither the station data nor the model data exhibits a statistically significant trend in MHW events for the  
200 overlapping period (Fig. 4i). But when all of the available model data from 1993–2022 is taken into account, the trend in MHW  
201 occurrences becomes significant at the 95 % level, with +0.64 MHWs per decade. Again, the number of events is positively  
202 correlated with annual mean temperature ( $R=0.58$ , Fig. 4j). The highest maximum MHW intensities were recorded in recent  
203 years (2016, 2018, 2021, 2022), with 2022 showing the highest intensity of any MHW, at 7.3 °C (model data) to 7.4 °C (station  
204 data) above the climatologically expected temperature (Fig. 4k,l, see also Fig. A2b). The cumulative MHW intensities show  
205 no clear trend or correlation with annual mean temperatures at this station (Fig. 4m,n). In terms of total MHW days, 2018  
206 shows the highest numbers (Fig. 4o), but otherwise no trend is detectable for this metric, though there is positive correlation  
207 with annual mean temperatures ( $R=0.56$ , Fig. 4p).

### 208 **3.2.2 Analysis of vertical MHW distribution at Northern Baltic**

209 At Northern Baltic, which is about 103 m deep and located in the Western Baltic Proper, the surface temperature has been  
210 measured continuously over several decades. Unfortunately, no quality-controlled temperature measurements exist for the

211 lower layers at this station. The model validation shows that, at other locations, the model represents temperatures generally  
212 well, both at the surface and in the lower layers. In order to obtain further insights into heat wave propagation towards the  
213 seafloor, we analyzed the MYP model data (product ref. no. 3 in Table 1) along the entire water column.

214 A seasonal SST signal is clearly visible in Fig. 5a. In general, the temperature tends to decrease with depth while the bottom  
215 temperature is relatively cold and uniform. In early summer (June), a so-called cold intermediate layer (CIL), defined as a  
216 minimum of temperature between the thermocline and the perennial halocline (Chubarenko et al., 2017; Dutheil et al., 2022),  
217 develops at a depth of 20–60 m and acts as a barrier between the surface and bottom water bodies. At Northern Baltic, the  
218 upper boundary of the CIL coincides with the mixed layer depth (MLD), which is depicted in Fig. 5b-c. Starting from around  
219 June, a layer of water with a significantly lower temperature than the climatological mean (up to  $-7^{\circ}\text{C}$  deviation) is found just  
220 below the MLD (Fig. 5b), which suggests that the CIL was significantly colder at this time in 2022. This also coincides with  
221 the onset of significantly higher temperatures at the surface compared to the climatological mean, though these were initially  
222 not high enough to result in a MHW (Fig. 5e). The elevated temperatures start with a significant temperature jump of  $5^{\circ}\text{C}$   
223 above the climatological mean, followed by abrupt and substantial decreases and increases in temperature over a short period.  
224 This eventually leads to a MHW which lasts for 15 days starting from the end of June and which contains a one-day extreme  
225 MHW (Category IV) event at a temperature of  $7.4^{\circ}\text{C}$  above the climatological mean, followed by a severe MHW (Category  
226 III) for another three days. Significantly high temperature deviations can also be observed at a depth of 10.8 m, i.e., at the  
227 MLD, after July 2nd, just after the Category IV MHW at the surface. However, these temperature deviations did not result in  
228 a MHW at this depth. Following the extreme heatwave event at the surface, a comparably weaker MHW can be detected in  
229 mid-August at both 0.5 m (Fig. 5e) and 10.8 m (Fig. 5f). Thus, this weaker MHW penetrates past the MLD into slightly deeper  
230 levels before reaching the comparably cold layer of water underneath.

231 As shown in Fig. 5c and Fig. 5d, the intensity of the MHW tends to decrease as the depth increases. Four MHWs in regions  
232 close to the seafloor (i.e., below 60 m) were detected during specific periods from February to April, September to October,  
233 and in December. These MHWs are mostly moderate, with temperatures reaching up to  $1.59^{\circ}\text{C}$  above the climatological mean.  
234 Only three days at the end of September can be classified as a Category II MHW in one specific depth-layer close to the  
235 seafloor. In the bottom-most depth-layer, the corresponding subsurface MHW is interrupted by five days of temperatures below  
236 the 90th percentile. However, as the temperatures are only slightly below the threshold and the MHW criteria are still met in  
237 the depth-layers above, one might still count this as one continuous MHW. Furthermore, Fig. 5c also shows isolated Category  
238 I MHWs at depths between 20 and 50 m.

#### 239 **4 Discussion and Conclusions**

240 During August and November 2022, record-warm sea surface temperatures were observed in substantial areas of the Baltic  
241 Sea proper. Large parts of the Baltic Sea exhibited the third-warmest to the warmest temperatures in summer and autumn



242 months since 1997. Both periods, in August and November, coincided with atmospheric temperature anomalies. Over the  
243 entire year of 2022, the distribution of quantity and intensity of MHWs within the Baltic Sea is twofold: up to seven individual  
244 MHW occurrences were recorded as well as simulated in the south-western part of the Baltic Sea, and as a result this region  
245 experienced the maximum number of total MHW days of anywhere in the Baltic Sea in 2022. In the northern Baltic Sea, the  
246 number of MHWs was lower, with some locations registering only one MHW; remarkably, however, this one MHW led to the  
247 highest mean and maximum MHW intensities in the Baltic Sea since the reanalysis started in 1993. In some areas in the  
248 Bothnian Bay, the Baltic Sea MYP revealed temperatures that exceeded 9 °C above the 90th percentile of the climatologically  
249 expected temperature values (Fig. 3d,e). This can be considered an extraordinarily high MHW intensity, since maximum SST  
250 anomalies above 5 °C have only been observed in about 5 % of the global ocean, and MHW intensities normally peak at 2.5 °C  
251 to 3.7 °C (Sen Gupta et al., 2020). In our case, the area in the Bothnian Bay experienced a short period with southerly winds  
252 and air temperatures up to 28 °C at the end of June 2022 (SMHI, 2023), which led to a short, but very intense MHW in the  
253 shallow areas of the Bay.

254 A significant increase in MHW occurrences is detectable over time at our two exemplary stations, of +0.73 MHW events per  
255 decade at LT Kiel and +0.64 MHW events per decade at Northern Baltic. Both MHW frequency and the total number of MHW  
256 days are statistically related to rising mean temperatures. This confirms that an increasing number of MHWs can be expected  
257 in the future in the Baltic Sea, too, due to global warming (Frölicher et al., 2018; Oliver et al., 2019). The adverse impact of  
258 MHWs on the ecosystem's various trophic levels has been widely documented (Smale et al., 2019; IPCC, 2022; Smith et al.,  
259 2023). The Baltic Sea, which has a relatively vulnerable ecosystem, could experience a significant negative impact from  
260 MHWs (Kauppi and Villnäs, 2022; Kauppi et al., 2023), and the analysis of subsurface MHWs opens up further potential ways  
261 to study their effects. At the Northern Baltic mooring station, MHWs were found at the surface, propagating into deeper layers  
262 until reaching the CIL, and some were also detected close to the seafloor. Isolated MHWs were also observed at depths of  
263 between 20 and 50 m. However, these are subject to higher uncertainty compared to the ones in the surface and bottom layers  
264 due to a higher uncertainty in modeling variability in the pycnocline (QuID; Panteleit et al., 2023). Among the possible reasons  
265 for the development of the four MHWs close to the seafloor at Northern Baltic could be vertical heat transport from the surface  
266 or a lateral transport of warmer water due to bottom currents, for example. However, a more detailed evaluation would be  
267 required to assess their precise cause.

268 Potential avenues for future studies include examining whether and how surface MHWs are able to propagate into the deeper  
269 water masses close to the halocline as well as examining the correlation between the strength (i.e., the classification category)  
270 of the MHW and its propagation into deeper water masses. At Northern Baltic, severe and extreme MHWs occurred at the  
271 surface when the CIL was particularly cold compared to the climatology. This therefore raises questions of whether a strong  
272 CIL might be linked to the development of MHWs at the surface and whether the one might even favor the development of  
273 the other. Additional studies could also focus on the positive feedback on the bottom temperature, as was observed in 2022. It  
274 might be interesting to determine if this phenomenon can also be found in other years and whether it is triggered by the

275 superposition of either lateral currents or MHWs or of both together. Understanding the effects that potentially lead to the  
276 vertical propagation of MHWs like those observed particularly in the late summer of 2022 will become increasingly crucial in  
277 order to evaluate how the already-increasing occurrences of surface MHWs may affect the ecosystem in subsurface layers.

## 278 **Appendix A1**

279 We apply a clustering approach to evaluate the precision of the hydrodynamic model. This technique offers insights into the  
280 overall accuracy of the model by grouping the errors. The clustering procedure employs the K-means algorithm, a type of  
281 unsupervised machine learning (Jain, 2010). The original explanation of this technique can be found in a study by Raudsepp  
282 and Maljutenko (2022). In our evaluation, all available data within the model's domain and simulation period are considered,  
283 even if the observation data is unevenly distributed or occasionally sparse. This strategy enables us to assess the model's quality  
284 at each specific location and time instance at which measurements have been acquired.

285 Initially, a two-dimensional error space ( $dS$ ,  $dT$ ) was established using simultaneously-measured temperature and salinity  
286 values as the foundation for clustering. Here,  $dS=(S_{\text{mod}}-S_{\text{obs}})$  and  $dT=(T_{\text{mod}}-T_{\text{obs}})$  represent the differences between the model  
287 ( $S_{\text{mod}}$  and  $T_{\text{mod}}$ ) and observed ( $S_{\text{obs}}$  and  $T_{\text{obs}}$ ) salinity and temperature, respectively. The dataset employed in this validation  
288 study was sourced from the EMODNET dataset compiled by SMHI (product ref. no. 4 in Table 1). It consists of a total of  
289 3,094,089 observations aligning with the simulation period of the Baltic Sea physics reanalysis (product ref. no. 3 in Table 1)  
290 and covering the years 1993 to 2022. For each observation, we extracted the nearest model values from the reanalysis dataset.  
291 The next stage involves choosing the number of clusters, and for simplicity we opted in advance for five clusters. Subsequently,  
292 the third step entails conducting K-means clustering on the two-dimensional errors. This clustering process is applied to the  
293 normalized errors achieved through separate normalization for temperature and salinity errors using the corresponding standard  
294 deviations. The K-means algorithm then identifies the centroids' positions within the error space for the predetermined number  
295 of clusters. These centroids' locations signify the bias of the error set for each cluster. In the fourth step, statistical metrics for  
296 non-normalized clustered errors are computed. Standard deviation (STD), root mean square deviation (RMSD) and the  
297 correlation coefficient are examples of common statistics that can be calculated for the parameters associated with each cluster.  
298 The fifth step involves examining the spatio-temporal distributions of errors associated with different clusters. During the  
299 creation of the error space, we retained the coordinates of each error point ( $dS$ ,  $dT$ )( $x$ ,  $y$ ), allowing us to map the errors of each  
300 cluster back onto the locations where the measurements were conducted. To achieve this, the model domain is partitioned into  
301 horizontal grid cells ( $i$ ,  $j$ ) of  $27 \times 27$  km<sup>2</sup> in size. Subsequently, the number of error points attributed to various clusters at each  
302 grid cell ( $i$ ,  $j$ ) is tallied. The total number of error points linked to the grid cell ( $i$ ,  $j$ ) is the sum of points from each cluster. The  
303 proportion of error points in each grid cell affiliated with cluster  $k$  is determined by the ratio of the number of error points of  
304 cluster  $k$  to the total number of error points in each grid cell.

305

306 Figure A1 displays the results of the K-means clustering for non-normalized errors. Table S1 presents the corresponding  
307 metrics. Within cluster  $k=5$ , the salinity and temperature values closely align with the observations, with a bias of  $dS=-$   
308  $0.40$  g/kg and  $dT=-0.02$  °C, respectively. This cluster encompasses 57 % of all data points. The points are distributed  
309 throughout the Baltic Sea and the great majority of them exceed 0.5 (Figure A1b). Clusters  $k=3$  and  $k=4$  exhibit relatively even  
310 spatial distributions across the Baltic Sea, accounting for 11 % and 8 % of the points, respectively. These clusters are  
311 particularly noteworthy due to their relatively high temperature biases and variability, both of which are crucial for the  
312 calculation of marine heatwaves. The clusters  $k=1$  and  $k=2$  represent points with low temperature but a high salinity error  
313 (Table A1). Spatially, these points are predominantly located in the southwestern Baltic Sea (Figure A1b), which points to the  
314 occasional underestimation or overestimation of the inflow/outflow salinity.  
315 Collectively, approximately 82 % of all validation points exhibit relatively low temperature bias, STD and RMSD (Table A1).  
316 The surface-layer validation shows that less than 10 % of comparison points have significant temperature errors (Figure A1c).  
317 Due to the low proportion of these validation points, we do not expect a significant impact on the determination of surface  
318 MHWs and their statistics. Below the surface layer, i.e., at depths ranging from 0.5–40 m, up to 25 % of the points correspond  
319 to clusters  $k=3$  and  $k=4$  (Figure A1c). Consequently, we anticipate that the model reanalysis data provides sufficiently accurate  
320 information for calculating subsurface MHWs and their statistics for the Baltic Sea.

### 321 **Data availability**

322 This study is based on public databases and the references are listed in Table 1.

### 323 **Author contribution**

324 The idea for and concept behind this chapter were formed by Anja Lindenthal, Claudia Hinrichs, Priidik Lagemaa, Helen E.  
325 Morrison and Urmas Raudsepp. The data curation was done by Eefke M. van der Lee and Tim Kruschke for the data from  
326 product ref. no. 1 in Table 1, by Claudia Hinrichs and Tabea R. Panteleit for the data from product ref. no. 2 in Table 1 and by  
327 Simon Jandt-Scheelke and Tabea R. Panteleit for the data from product ref. no. 3 in Table 1. The formal analyses of the datasets  
328 and the resulting investigations were performed by Anja Lindenthal, Claudia Hinrichs, Simon Jandt-Scheelke, Tim Kruschke  
329 and Tabea R. Panteleit. The k-means model validation was performed by Urmas Raudsepp and Ilja Maljutenko. Claudia  
330 Hinrichs, Simon Jandt-Scheelke, Ilja Maljutenko, Tim Kruschke and Tabea R. Panteleit were responsible for the visualization  
331 of the data. Anja Lindenthal, Claudia Hinrichs, Simon Jandt-Scheelke, Tim Kruschke, Eefke M. van der Lee, Tabea R. Panteleit  
332 and Urmas Raudsepp were involved in the original draft preparation. The final manuscript was reviewed and edited by Claudia  
333 Hinrichs, Priidik Lagemaa, Helen E. Morrison and Urmas Raudsepp with contributions from all co-authors.

334 **Competing interests**

335 The authors declare that they have no conflict of interest.

336 **Funding**

337 This work is supported by the Copernicus Marine Service for the Baltic Sea Monitoring and Forecasting Center (21002L2-  
338 COP-MFC BAL-5200).

339 **References**

340 Belkin, I. M.: Rapid warming of large marine ecosystems. *Progress in Oceanography*, 81(1-4), 207-213,  
341 <https://doi.org/10.1016/j.pocean.2009.04.011>, 2009.

342 Buga, L., Sarbu, G., Fryberg, L., Magnus, W., Wesslander, K., Gatti, J., Leroy, D., Iona, S., Larsen, M., Koefoed Rømer, J.,  
343 Østrem, A. K., Lipizer, M., and Giorgetti A.: EMODnet Chemistry Eutrophication and Acidity aggregated datasets v2018,  
344 EMODnet, Thematic Lot no. 4/SI2.749773, <https://doi.org/10.6092/EC8207EF-ED81-4EE5-BF48-E26FF16BF02E>, 2018.

345 Cheng, L., von Schuckmann, K., Abraham, J. P., et al.: Past and future ocean warming, *Nature Reviews Earth and*  
346 *Environment*, 3(11), 776-794, <https://doi.org/10.1038/s43017-022-00345-1>, 2022.

347 Chubarenko, I. P., Demchenko, N. Y., Esiukova, E. E., Lobchuk, O. I., Karmanov, K. V., Pilipchuk, V. A., Isachenko, I. A.,  
348 Kuleshov, A. F., Chugaevich, V. Y., Stepanova, N. B. et al.: Spring thermocline formation in the coastal zone of the  
349 southeastern Baltic Sea based on field data in 2010–2013. *Oceanology*, 57, 632–638,  
350 <https://doi.org/10.1134/S000143701705006X>, 2017.

351 Copernicus Climate Change Service/ECMWF, <https://climate.copernicus.eu/surface-air-temperature-august-2022>, last access:  
352 11 July 2023, 2022a.

353 Copernicus Climate Change Service/ECMWF, <https://climate.copernicus.eu/surface-air-temperature-november-2022>, last  
354 access: 11 July 2023, 2022b.

355 Dutheil, C., Meier, H. E. M., Gröger, M., Börgel, F.: Warming of Baltic Sea water masses since 1850, *Climate Dynamics*,  
356 <https://doi.org/10.1007/s00382-022-06628-z>, 2022.

357 EU Copernicus Marine Service Product: Global Ocean- In-Situ Near-Real-Time Observations, Mercator Ocean International,  
358 [data set], <https://doi.org/10.48670/moi-00036>, 2022a.

359 EU Copernicus Marine Service Product: Baltic Sea - L3S Sea Surface Temperature Reprocessed, Mercator Ocean  
360 International, [data set], <https://doi.org/10.48670/moi-00312>, 2022b.

361 EU Copernicus Marine Service Product: Baltic Sea Physics Reanalysis, Mercator Ocean International, [data set],  
362 <https://doi.org/10.48670/moi-00013>, 2023.

363 EUMETSAT, AVHRR Factsheet, Doc.No.: EUM/OPS/DOC/09/5183, <https://www.eumetsat.int/media/39253>, 2015.

364 Frölicher, T. L., Fischer, E. M., Gruber, N.: Marine heatwaves under global warming, *Nature*, 560, 360–364,  
365 <https://doi.org/10.1038/s41586-018-0383-9>, 2018.

366 Giorgetti, A., Lipizer, M., Molina Jack, M. E., Holdsworth, N., Jensen, H. M., Buga, L., Sarbu, G., Iona, A., Gatti, J., Larsen,  
367 M., and Fyrberg, L.: Aggregated and Validated Datasets for the European Seas: The Contribution of EMODnet Chemistry,  
368 *Front. Mar. Sci.*, 7, 583657, <https://doi.org/10.3389/fmars.2020.583657>, 2020.

369 Goebeler, N., Norkko, A., Norkko, J.: Ninety years of coastal monitoring reveals baseline and extreme ocean temperatures are  
370 increasing off the Finnish coast, *Commun. Earth Environ.*, 3, 215, <https://doi.org/10.1038/s43247-022-00545-z>, 2022.

371 Gröger, M., Placke, M., Meier, H. E. M., Börgel, F., Brunnabend, S.-E., Dutheil, C., Gräwe, U., Hieronymus, M., Neumann,  
372 T., Radtke, H., Schimanke, S., Su, J., Väli, G.: The Baltic Sea Model Intercomparison Project (BMIP) – a platform for model  
373 development, evaluation, and uncertainty assessment, *Geosci. Model Dev.*, 15, 8613–8638, [https://doi.org/10.5194/gmd-15-](https://doi.org/10.5194/gmd-15-8613-2022)  
374 [8613-2022](https://doi.org/10.5194/gmd-15-8613-2022), 2022.

375 Gurvan, M., Bourdallé-Badie, R., Chanut, J., Clementi, E., Coward, A., Ethé, C., Iovino, D., Lea, D., Lévy, C., Lovato, T.,  
376 Martin, N., Masson, S., Mocavero, S., Rousset, C., Storkey, D., Vancoppenolle, M., Müeller, S., Nurser, G., Bell, M., Samson,  
377 G.: NEMO ocean engine. In *Notes du Pôle de modélisation de l'Institut Pierre-Simon Laplace (IPSL) (v4.0, Number 27)*.  
378 Zenodo. <https://doi.org/10.5281/zenodo.3878122>, 2019.

379 Hobday, A. J., Alexander, L. V., Perkins, S. E., Smale, D. A., Straub, S. C., et al.: A hierarchical approach to defining marine  
380 heatwaves, *Prog. Oceanogr.*, 141, 227–38, <https://doi.org/10.1016/j.pocean.2015.12.014>, 2016.

381 Hobday, A. J., Oliver, E. C. J., Sen Gupta, A., Benthuisen, J. A., Burrows, M. T., Donat, M. G., Holbrook, N. J., Moore, P. J.,  
382 Thomsen, M. S., Wernberg, T., Smale, D. A.: Categorizing and naming marine heatwaves, *Oceanography*, 31(2), 162–173,  
383 <https://doi.org/10.5670/oceanog.2018.205>, 2018.

384 Holbrook, N.J., Scannell, H.A., Sen Gupta, A., Benthuisen, J.A., Feng, M., Oliver, E.C., Alexander, L.V., Burrows, M.T.,  
385 Donat, M.G., Hobday, A.J. and Moore, P.J.. A global assessment of marine heatwaves and their drivers. *Nature*  
386 *communications*, 10(1), p.2624. <https://doi.org/10.1038/s41467-019-10206-z>. 2019.

387 ICES Bottle and low-resolution CTD dataset, Extractions 22 DEC 2013 (for years 1990-20012), 25 FEB 2015 (for year 2013),  
388 13 OCT 2016 (for year 2015), 15 JAN 2019 (for years 2016-2017), 22 SEP 2020 (for year 2018), 10 MAR 2021 (for years  
389 2019-202), 28 FEB 2022 (for year 2021), ICES, Copenhagen, 2022.

390 In Situ TAC partners: EU Copernicus Marine Service Product User Manual for the Global Ocean- In-Situ Near-Real-Time  
391 Observations Product, INSITU\_GLO\_PHYBGCWAV\_DISCRETE\_MYNRT\_013\_030, Issue 1.14, Mercator Ocean  
392 International, <https://catalogue.marine.copernicus.eu/documents/PUM/CMEMS-INS-PUM-013-030-036.pdf>, last access: 12  
393 April 2023, 2022.

394 IPCC: Climate Change 2022: Impacts, Adaptation, and Vulnerability. Contribution of Working Group II to the Sixth  
395 Assessment Report of the Intergovernmental Panel on Climate Change, eds.: Pörtner, H.-O., Roberts, D. C., Tignor, M.,  
396 Poloczanska, E. S., Mintenbeck, K., Alegría, A., Craig, M., Langsdorf, S., Löschke, S., Möller, V., Okem, A., Rama, B.,  
397 Cambridge University Press, Cambridge, UK and New York, NY, USA, 3056 pp., <https://doi.org/10.1017/9781009325844>,  
398 2022.

399 Jain, A. K.: Data clustering: 50 years beyond K-means, *Pattern Recognition Letters*, 31(8), 651-666,  
400 <https://doi.org/10.1016/j.patrec.2009.09.011>, 2010.

401 Kauppi, L., Villnäs, A.: Marine heatwaves of differing intensities lead to distinct patterns in seafloor functioning, *Proceedings*  
402 *of the Royal Society B: Biological Sciences*, 289(1986), 20221159, <https://doi.org/10.1098/rspb.2022.1159>, 2022.

403 Kauppi, L., Göbeler, N., Norkko, J., Norkko, A., Romero-Ramirez, A., Bernard, G.: Changes in macrofauna bioturbation  
404 during repeated heatwaves mediate changes in biogeochemical cycling of nutrients, *Frontiers in Marine Science*, 9, 1070377,  
405 <https://doi.org/10.3389/fmars.2022.1070377>, 2023.

406 Minnett, P. J., Alvera-Azcárate, A., Chin, T. M., Corlett, G. K., Gentemann, C. L., Karagali, I., Li, X., Marsouin, A., Marullo,  
407 S., Maturi, E., Santoleri, R., Saux Picart, S., Steele, M., Vazquez-Cuervo, J.: Half a century of satellite remote sensing of sea-

408 surface temperature, Remote Sensing of Environment, 233, 111366, ISSN 0034-4257,  
409 <https://doi.org/10.1016/j.rse.2019.111366>, 2019.

410 Oliver, E. C. J.: marineHeatWaves v0.16, github [code], <https://github.com/ecjoliver/marineHeatWaves>, 2016.

411 Oliver, E. C. J.: Mean warming not variability drives marine heatwave trends, Clim. Dyn., 53, 1653–1659,  
412 <https://doi.org/10.1007/s00382-019-04707-2>, 2019.

413 Panteleit, T., Verjovkina, S., Jandt-Scheelke, S., Spruch, L. and Huess, V.: EU Copernicus Marine Service Quality Information  
414 Document for the Baltic Sea Physics Reanalysis Product, BALTICSEA\_MULTIYEAR\_PHY\_003\_011, Issue 4.0, Mercator  
415 Ocean International, <https://catalogue.marine.copernicus.eu/documents/QUID/CMEMS-BAL-QUID-003-011.pdf>, last  
416 access: 12 April 2023, 2023.

417 Raudsepp, U., Maljutenko, I., Haapala, J., Männik, A., Verjovkina, S., Uiboupin, R., von Schuckmann, K., Mayer, M.: Record  
418 high heat content and low ice extent in the Baltic Sea during winter 2019/20. In: Copernicus Ocean State Report, Issue 6,  
419 Journal of Operational Oceanography, 15:sup1, s175–s185, <https://doi.org/10.1080/1755876X.2022.2095169>, 2022.

420 Raudsepp, U., Maljutenko, I.: A method for assessment of the general circulation model quality using K-means clustering  
421 algorithm: a case study with GETM v2.5, Geosci Model Dev., 15, 535–551, <https://doi.org/10.5194/gmd-15-535-2022>, 2022.

422 Ringgaard, I., Korabel, V., Spruch, L., Lindenthal, A. and Huess, V.: EU Copernicus Marine Service Product User Manual for  
423 the Baltic Sea Physics Reanalysis Product, BALTICSEA\_MULTIYEAR\_PHY\_003\_011, Issue 1.0, Mercator Ocean  
424 International, [https://catalogue.marine.copernicus.eu/documents/PUM/CMEMS-BAL-PUM-003-011\\_012.pdf](https://catalogue.marine.copernicus.eu/documents/PUM/CMEMS-BAL-PUM-003-011_012.pdf), last access: 12  
425 April 2023, 2023.

426 Sen Gupta, A., Thomsen, M., Benthuyesen, J.A. et al.: Drivers and impacts of the most extreme marine heatwave events, Sci  
427 Rep 10, 19359, <https://doi.org/10.1038/s41598-020-75445-3>, 2020.

428 She, J., Su, J., Zinck, A.-S.: Anomalous surface warming in the Baltic Sea in summer 2018 and mechanism analysis, In:  
429 Copernicus Marine Service Ocean State Report, Issue 4, Journal of Operational Oceanography, 13:sup1, s125–s132;  
430 <https://doi.org/10.1080/1755876X.2020.1785097>, 2020.

431 Smale, D. A., Wernberg, T., Oliver, E. C. J., et al.: Marine heatwaves threaten global biodiversity and the provision of  
432 ecosystem services, Nature Climate Change, 9(4), 306-312, <https://doi.org/10.1038/s41558-019-0412-1>, 2019.

433 SMHI: Baltic Sea – Eutrophication and Acidity aggregated datasets 1902/2017 v2018, Aggregated datasets were generated in  
434 the framework of EMODnet Chemistry III, under the support of DG MARE Call for Tender EASME/EMFF/2016/006 – lot4,  
435 EMODnet Chemistry [data set], <https://doi.org/10.6092/595D233C-3F8C-4497-8BD2-52725CEFF96B>, 2019.

436 SMHI: Meteorological observations [data set], air temperature, station number 140480 (Umeå Flygplats),  
437 [https://www.smhi.se/data/meteorologi/ladda-ner-meteorologiska-](https://www.smhi.se/data/meteorologi/ladda-ner-meteorologiska-observationer/#param=airtemperatureInstant,stations=core,stationid=140480)  
438 [observationer/#param=airtemperatureInstant,stations=core,stationid=140480](https://www.smhi.se/data/meteorologi/ladda-ner-meteorologiska-observationer/#param=airtemperatureInstant,stations=core,stationid=140480), last access: 19 Dec 2023, 2023.

439 Smith, K. E., Burrows, M. T., Hobday, A. J., King, N. G., Moore, P. J., Gupta, A. S., Thomsen, M. S., Wernberg, T., Smale,  
440 D. A.: Biological Impacts of Marine Heatwaves. *Annual Review of Marine Science*, 15 (1), 119–145.  
441 <https://doi.org/10.1146/annurev-marine-032122-121437>, 2023.

442 Sun, D., Jing, Z., Li, F., Wu, L.: Characterizing global marine heatwaves under a spatio-temporal framework, *Progress in*  
443 *Oceanography*, 211, 102947, <https://doi.org/10.1016/j.pocean.2022.10294>, 2023.

444 The BACC Author Team: Assessment of Climate Change for the Baltic Sea Basin, Springer Berlin, Heidelberg, p. 88,  
445 <https://doi.org/10.1007/978-3-540-72786-6>, 2008.

446 Väli, G., Meier, H. M., Elken, J.: Simulated halocline variability in the Baltic Sea and its impact on hypoxia during 1961–  
447 2007, *J. Geophys. Res. Oceans*, 118, 6982-7000, <https://doi.org/10.1002/2013JC009192>, 2013.

448 Wehde, H., Schuckmann, K. V., Pouliquen, S., Grouazel, A., Bartolome, T., Tintore, J., De Alfonso Alonso-Munoyerro, M.,  
449 Carval, T., Racapé, V. and the INSTAC team: EU Copernicus Marine Service Quality Information Document for the Global  
450 Ocean- In-Situ Near-Real-Time Observations Product, INSITU\_GLO\_PHYBGCWAV\_DISCRETE\_MYNRT\_013\_030,  
451 Issue 2.2, Mercator Ocean International, [https://catalogue.marine.copernicus.eu/documents/QUID/CMEMS-INS-QUID-013-](https://catalogue.marine.copernicus.eu/documents/QUID/CMEMS-INS-QUID-013-030-036.pdf)  
452 [030-036.pdf](https://catalogue.marine.copernicus.eu/documents/QUID/CMEMS-INS-QUID-013-030-036.pdf), last access: 12 April 2023, 2022.

453 WMO: State of the Global Climate 2022, WMO-No. 1316, World Meteorological Organization, 2023, 48 pp., 2023.

454 Zhao, Z., Marin, M.: A MATLAB toolbox to detect and analyze marine heatwaves, *Journal of Open Source Software*, 4(33),  
455 1124, <https://doi.org/10.21105/joss.01124>, 2019.



456 **Tables**

457

458 **Table 1: Product Table**

Product ref. no.	Product ID & type	Data access	Documentation
1	BSH Sea Surface Temperature (AVHRR/3); Satellite data	Upon request; overview and contact data via <a href="https://www.bsh.de/EN/TOPICS/Monitoring_systems/Remote_sensing/remote_sensing_node.html">https://www.bsh.de/EN/TOPICS/Monitoring_systems/Remote_sensing/remote_sensing_node.html</a>	<a href="https://www.bsh.de/DE/THEMEN/Beobachtungssysteme/Fernerkundung/fernerkundung_node.html">https://www.bsh.de/DE/THEMEN/Beobachtungssysteme/Fernerkundung/fernerkundung_node.html</a>
2	INSITU_GLO_PHYBGCWAV_DISCRETE_MYNRT_013_030; In-Situ Near-Real-Time Observations	<a href="#">EU Copernicus Marine Service Product (2022a)</a>	Quality Information Document (QUID): <a href="#">Wehde et al. (2022)</a> Product User Manual (PUM): <a href="#">In Situ TAC partners (2022)</a>
3	BALTICSEA_MULTIYEAR_PHY_003_011; Numerical models	<a href="#">EU Copernicus Marine Service Product (2023)</a>	Quality Information Document (QUID): <a href="#">Panteleit et al. (2023)</a> Product User Manual (PUM): <a href="#">Ringgaard et al. (2023)</a>
4	EMODNET_CHEMISTRY_Baltic_Sea_aggregated_eutrophication_and_acidity_datasets_1902-2017_v2018; Observations	SMHI (2019)	Buga et al. (2018), Giorgetti et al. (2020)

459

460 **Table 2: Pearson correlation coefficients from linear regression between the MHW metrics computed from the station data and the**  
461 **model data at the stations Lighthouse Kiel and Northern Baltic.**

Station	common climatology period	MHW count	MHW max intensity	MHW cumulative intensity	total MHW days
Lighthouse Kiel	1993-2021	0.82	0.88	0.66	0.93
Northern Baltic	1997-2021	0.74	0.89	0.82	0.94

462

463

464  
465  
466

**Table 3: Statistical MHW parameter values in various subregions of the Baltic Sea for 2022 based on the model data from the Baltic Sea MYP (product ref. no. 3 in Table 1) using daily values of SST between 1st January 1993 and 31st December 2022. The climatological period covers the years 1993 to 2021.**

	Kattegat	Inner Danish Straits	Western Baltic	Baltic Proper	Gulf of Riga	Gulf of Finland	Archipelago Sea	Bothnian Sea	Bothnian Bay
Cumulative intensity of longest MHW / °C days	81.5	63.8	64	79.4	63	66.5	61.1	119.3	85.1
Mean intensity / °C	3.6	3.5	3.8	5.3	4.9	5.8	4.5	6.4	6.5
Duration of longest MHW / days	24	29	26	32	17	17	21	31	20
Number of MHWs (modal) per year	1-6 (3)	2-7 (4)	2-7 (5)	1-7 (3)	1-4 (3)	1-4 (2)	2-4 (3)	1-6 (2)	1-5 (2)
Maximum intensity / °C	4.5	4.2	4.6	7.3	5.9	6.8	5.1	8.6	9.6
Total days of MHW conditions / days	56	86	94	79	50	48	55	63	47

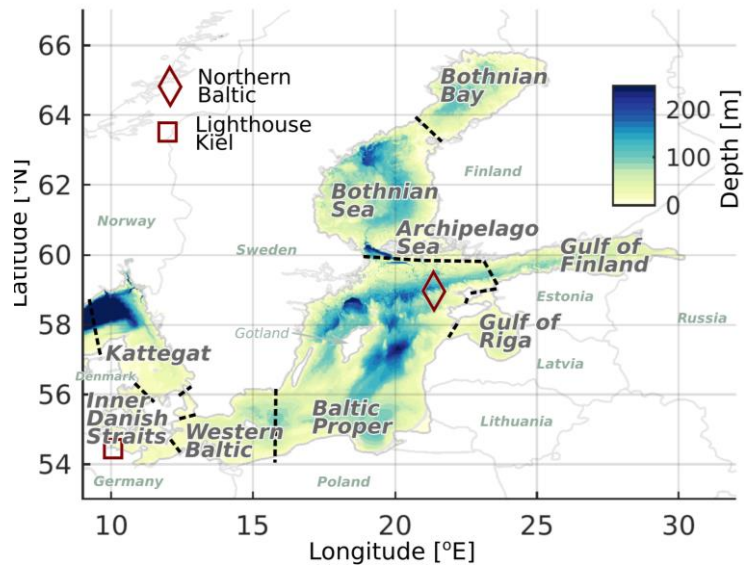
467

468  
469

**Table A1: The share (%), bias, root-mean-square error (RMSE), standard deviation (SD), and correlation coefficient (Corr) for each of the five clusters.**

k	Shares %	Bias		SD		RMSE		Corr		
		dS (g/kg)	dT (°C)	dS (g/kg)	dT (°C)	S (g/kg)	T (°C)	S	T	dSdT
1	18.6	-4.14	-0.26	1.80	0.85	4.51	0.89	0.90	0.78	-0.09
2	7.4	3.53	0.39	2.16	1.06	4.14	1.13	0.93	0.75	-0.11
3	10.5	-0.62	2.58	2.12	1.28	2.21	2.88	0.97	0.58	-0.06
4	6.3	0.27	-2.29	1.97	1.21	1.99	2.59	0.95	0.71	-0.14
5	57.2	-0.40	-0.02	0.83	0.54	0.92	0.54	0.99	0.89	0.07

470



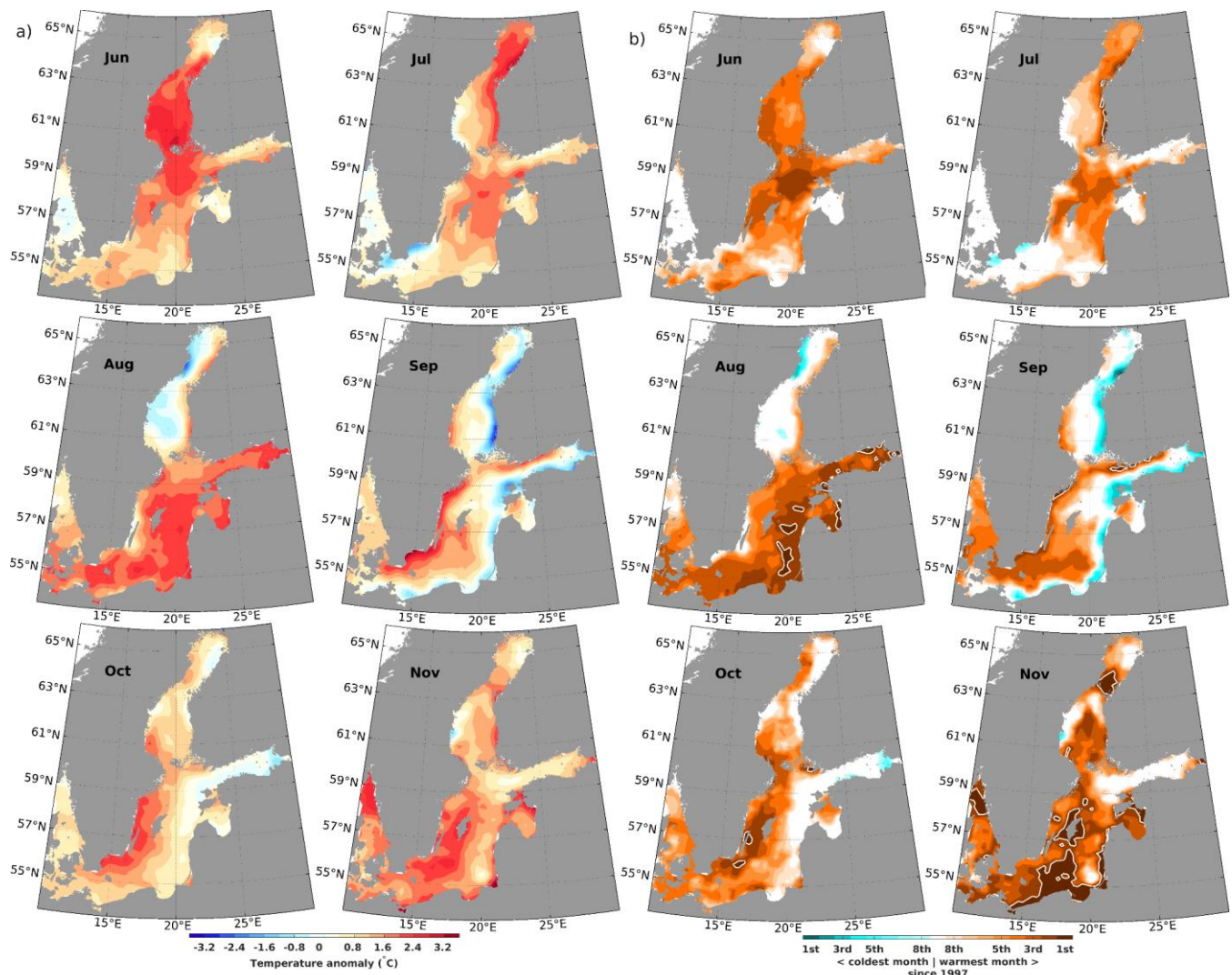
472

473

474

**Figure 1: Map of the Baltic Sea with relevant locations mentioned in the study. Boundaries between subregions are marked with dashed lines.**

475



476

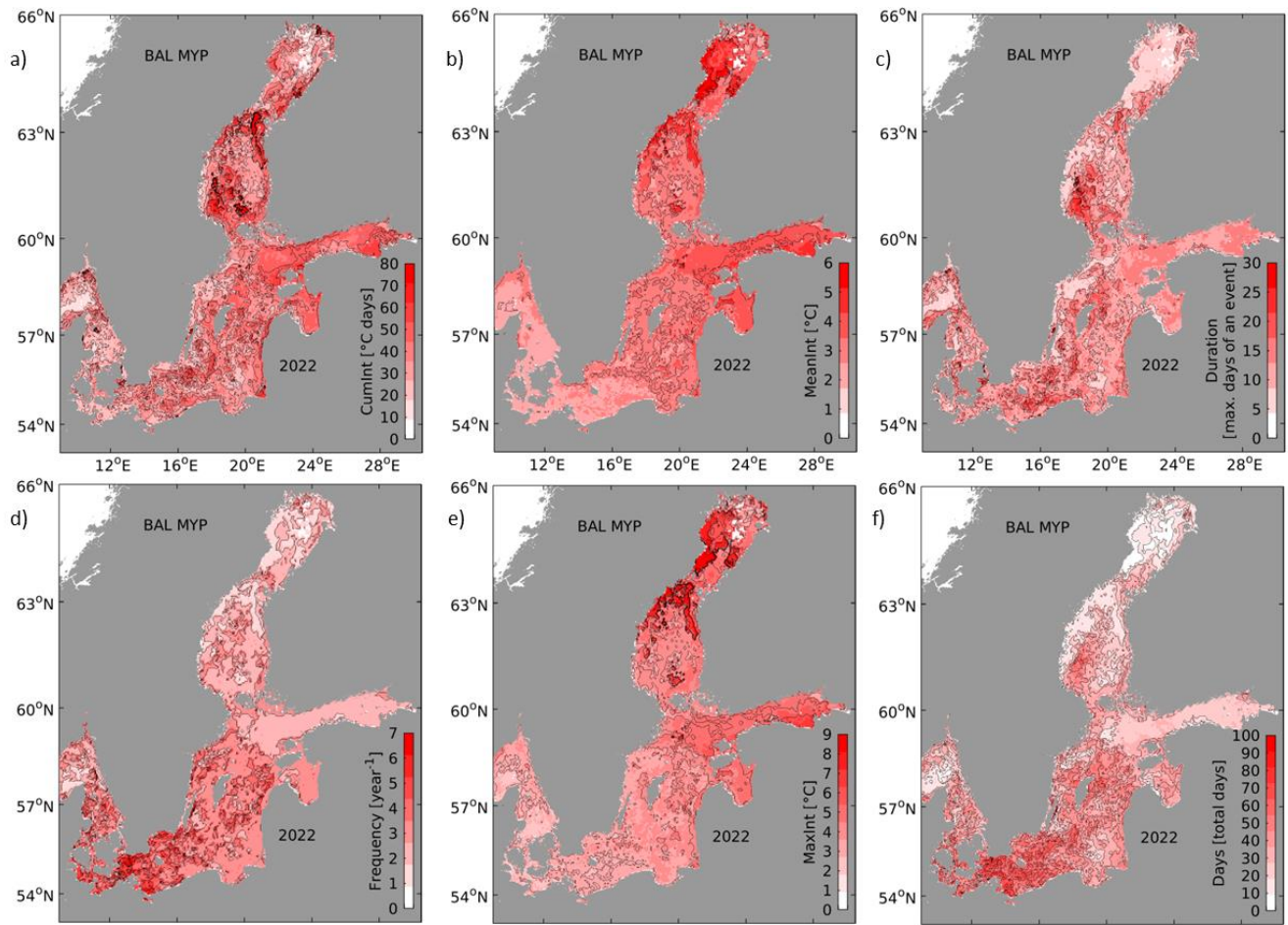
477

478

479

480

**Figure 2: Anomalies (difference to climatology of 1997-2021) of SST for the Baltic Sea according to the BSH SST analysis (product ref. no 1 in Table 1) during the summer and autumn months in 2022 (a) and ranks of these SST anomalies (b) when compared to the full dataset starting in 1997. In (b), brownish (cyan) colors denote anomalies belonging to the warmest (coldest) eight anomalies found since 1997. Record warm anomalies (rank 1) are highlighted by white contours.**



481

482

483

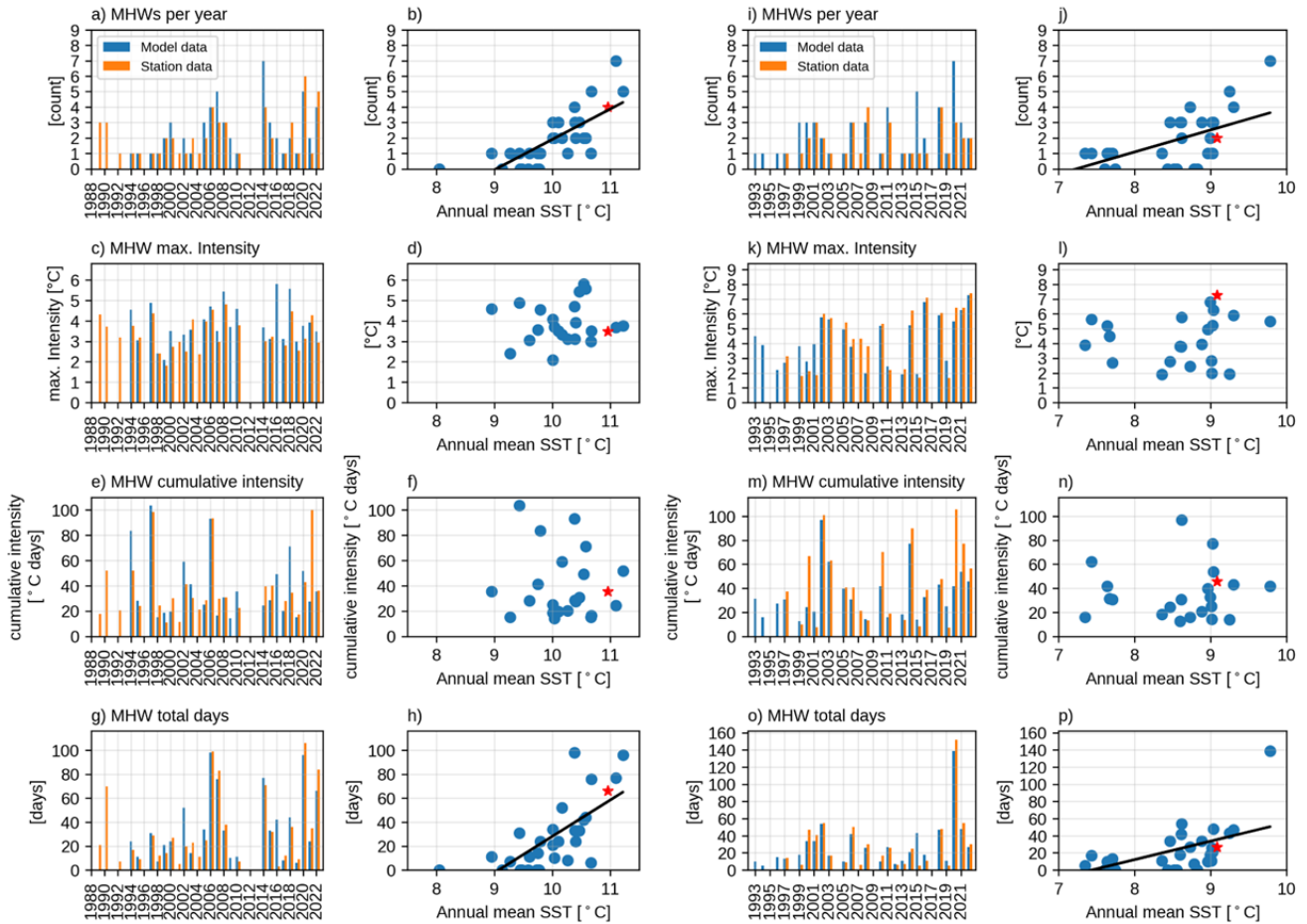
484

485

**Figure 3: Statistical metrics of MHWs in 2022 in the Baltic Sea based on SST data of the Baltic Sea MYP (product ref. no. 3 in Table 1) with the climatological period covering the years 1993 to 2021 - (a) cumulative intensity of the longest heatwave, (b) mean intensity, (c) duration of the longest heatwave, (d) number of heatwaves during 2022, (e) maximum intensity during the longest heatwave, (f) summed up days of all heatwave during 2022. The definition of these metrics follows [Hobday et al. \(2016\)](#).**

## LT Kiel

## Northern Baltic



486

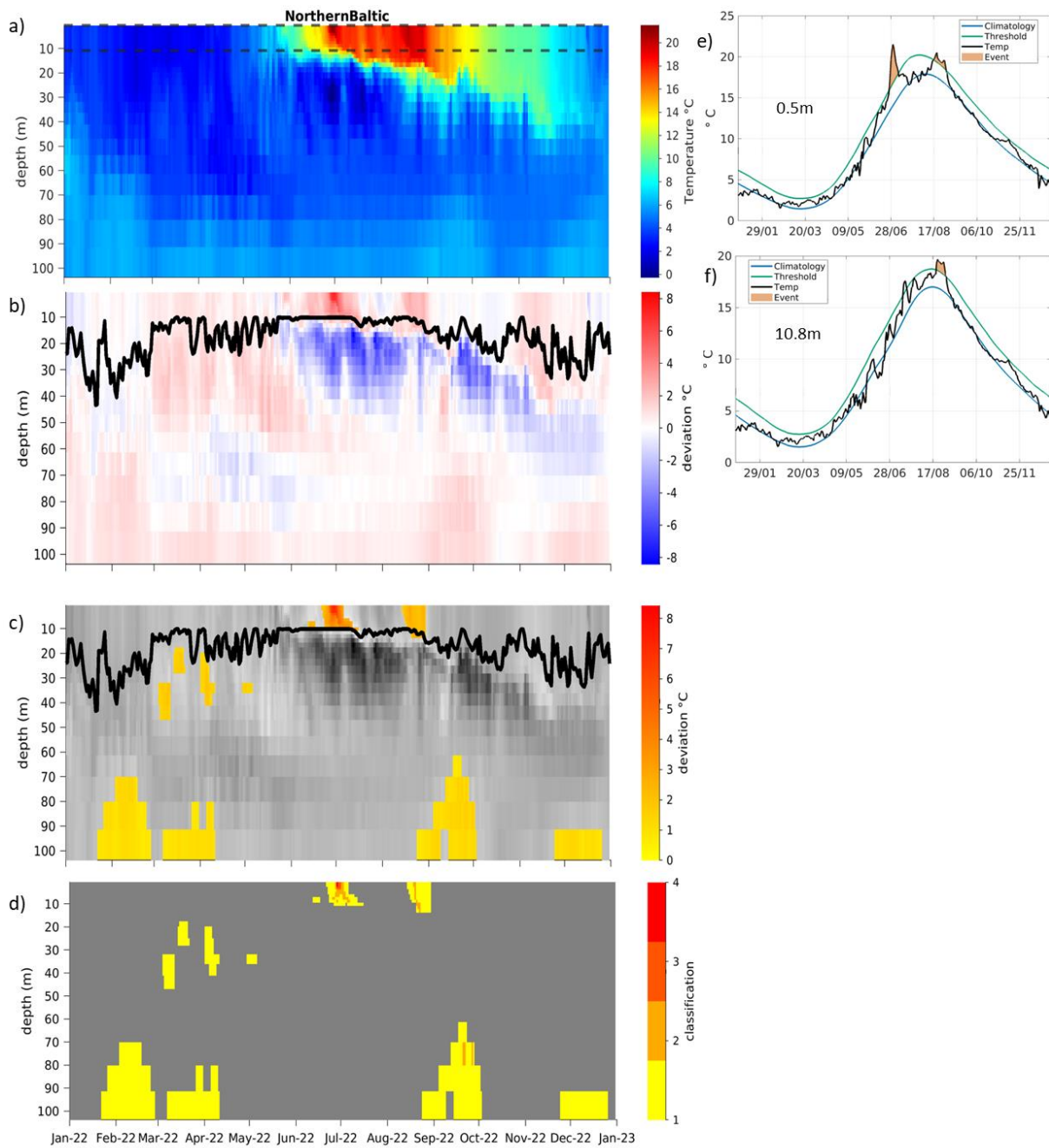
487

488

489

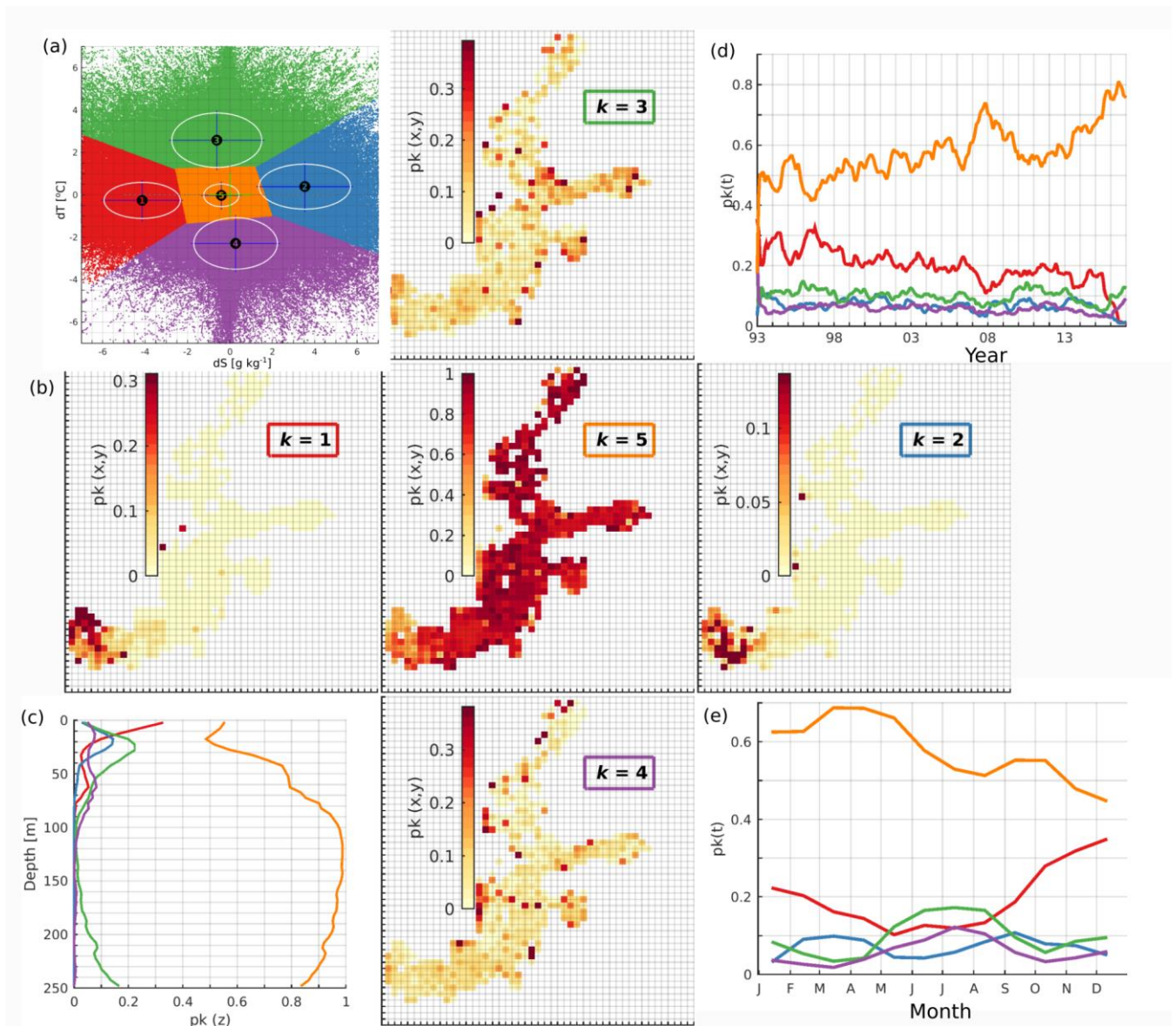
490

**Figure 4: Comparison and time series of annual MHW metrics (a,i: MHW events; c,k: maximum intensity [°C]; e,m: cumulative intensity [°C days]; g,o: MHW days) for station data (orange bars) and model data (blue bars) at the stations LT Kiel (left) and Northern Baltic (right). The MHW metrics from the model are plotted against the annual mean SST at that station with the year 2022 marked in red. Statistically significant (95 %) correlations are indicated with a black line.**



491

492 **Figure 5:** Hovmöller diagrams show absolute water temperature (a), temperature deviation between the climatology and the MYP  
 493 data for 2022 (b) and MHWs (c) and their classifications (d, 1-moderate, 2-strong, 3-severe, 4-extreme) including the mixed layer  
 494 depth as the thick black line (b and c) at Northern Baltic based on the Baltic Sea MYP (product ref. no. 3 in Table 1). The time series  
 495 on the right (e-f) are located at the vertical positions marked as dashed lines in (a) and show temperature (black), climatology (blue),  
 496 90<sup>th</sup> percentile threshold for MHW analysis (green) and MHWs (red shading) based on model data at depths of 0.5 m (e) and 10.8 m  
 497 (f). The period used for the climatology is 1993-2021.

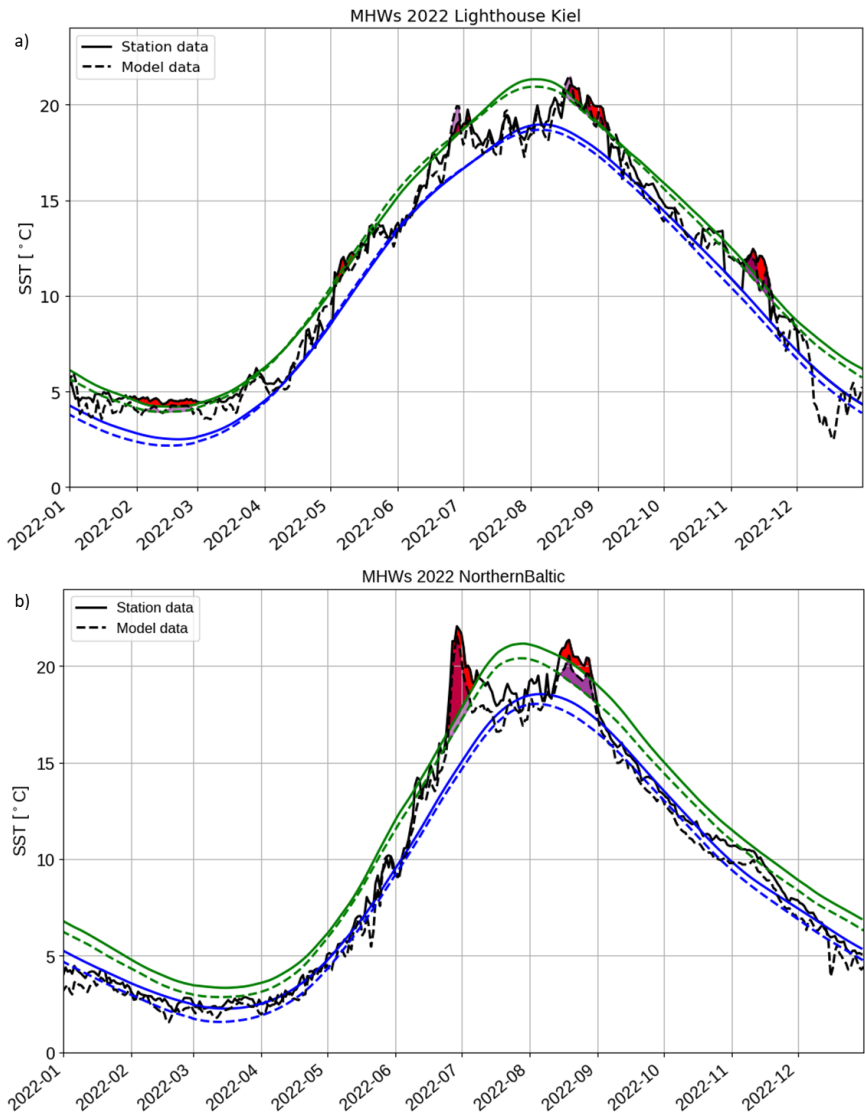


498

499  
500

**Figure A1:** Distribution of normalized error clusters for  $k=5$  (a). The spatial distribution (b, shaded sub-plots), vertical distribution (c), temporal distribution (d), and seasonal distribution (e) of the share of error points belonging to the five different clusters.





501

502 **Figure A2: Comparison of station data with model data at (a) LT Kiel (product ref. no. 2 and 3 in Table 1), (b) Northern Baltic (K.**  
 503 **Hedi, FMI, pers. communication and product ref. no. 3 in Table 1). The dashed lines correspond to the model, while the continuous**  
 504 **lines correspond to the station data. In blue, the climatological mean is shown. The green lines show the 90th percentile threshold**  
 505 **for MHW detection and the black lines are the respective 2022 temperature data. The purple (model data) and red (station data)**  
 506 **marked areas show the detected MHWs in 2022. The reference period is 1993-2021 for LT Kiel (a) and 1997-2021 for Northern**  
 507 **Baltic (b).**